STM JOURNALS

Journal of
Polymer & Composites

ISSN: 2321-2810 (Online)
ISSN: 2321-8525 (Print)
Volume 14, Issue 1, 2026
DOI (Journal): 10.37591/JoPC

https://journals.stmjournals.com/jopc

Research JoPC

Development of a Durable Superhydrophobic EP/PDMS Coating Reinforced with Micro-$CaCO_3$ and Nano-ZnO for Enhanced Corrosion Protection and Multifunctional Performance on Carbon Steel

Nurul Nabila Binti Mohd Din [1], Norhasnidawani Binti Johari [2,*], Mohd Aidy Faizal Bin Johari [3], Noor Azlina Binti Hassan [4], Abd Halim Bin Md Ali [5], Rizal Arifin [6]

Abstract

Balancing exceptional multifunctional performance with mechanical robustness in micro-nano composite films remains a significant challenge for practical applications. In this work, a superhydrophobic coating reinforced with micro-$CaCO_3$ and nano-ZnO particles was fabricated through a versatile single-step brushing method. The optimized EP/PDMS@micro-$CaCO_3$/nano-ZnO coating achieved a water contact angle (WCA) of 173.54° ± 2.53° and a sliding angle (SA) of 1.50° ± 1.12°. Owing to its carefully engineered micro-nano hierarchical structure, the coating exhibited outstanding friction coefficient reduction efficiency of 76.2% and mechanical durability Furthermore, the coating demonstrated superior anti-pollution properties, self-cleaning capability, substrate versatility, thermal stability, and anti-icing performance. Electrochemical evaluations revealed that the coating provided corrosion protection efficiency exceeding 99% in a 3.5 wt% NaCl solution, indicating substantially enhanced corrosion resistance. The results demonstrate that the modified $CaCO_3$ - ZnO nanoparticles do not merely function as surface roughness generators but actively reinforce the polymer matrix by enhancing interfacial bonding and suppressing nanoparticle pull-out during mechanical abrasion. The incorporation of PDMS further contributes to stress absorption while maintaining low surface energy, enabling sustained superhydrophobicity under repeated mechanical, chemical, and thermal exposure. This study provides new mechanistic insight into the durability of $CaCO_3$-based superhydrophobic coatings and shifts the focus of superhydrophobic coating design from short-term repellency performance toward durability-driven material engineering. The findings offer a viable strategy for developing robust superhydrophobic coatings suitable for marine atmospheric corrosion protection applications. The intrinsic properties of micro-$CaCO_3$/nano-ZnO particles, along with their highly ordered assembly within the coating, present a promising and effective strategy for the design and fabrication of multifunctional, all-in-one composite films.

***Author for Correspondence**
Norhasnidawani Binti Johari
E-mail id: Evabella2921@gmail.com

[1,3]Postgraduate Student, Engineering Materials and Structures (EMaSt), Malaysia-Japan International Institute of Technology (MJIIT), Universiti Teknologi Malaysia (UTM), Jalan Sultan Yahya Petra, Kuala Lumpur, Malaysia
[2]Senior Lecturer, Department of Mechanical Precision Engineering (MPE), Malaysia-Japan International Institute of Technology (MJIIT), Universiti Teknologi Malaysia (UTM), Jalan Sultan Yahya Petra, Kuala Lumpur, Malaysia
[4]Associate Professor, Department of Manufacturing and Materials Engineering, Faculty of Engineering, International Islamic University Malaysia (IIUM), Jalan Gombak, Kuala Lumpur, Malaysia
[5]Senior Lecturer, Malaysia-Japan Advanced Research Centre (MJARC), Malaysia- Japan International Institute of Technology (MJIIT), Universiti Teknologi Malaysia (UTM), Jalan Sultan Yahya Petra, Kuala Lumpur, Malaysia
[6]Senior Lecturer, Faculty of Engineering, Universitas Muhammadiyah Ponorogo, Jl. Budi Utomo No. 10 Ponorogo, Indonesia

Received Date: January 08, 2026
Accepted Date: January 16, 2026
Published Date: January 27, 2026

Citation: Nurul Nabila Binti Mohd Din, Norhasnidawani Binti Johari, Mohd Aidy Faizal Bin Johari, Noor Azlina Binti Hassan, Abd Halim Bin Md Ali, Rizal Arifin. Development of a Durable Superhydrophobic EP/PDMS Coating Reinforced with Micro-$CaCO_3$ and Nano-ZnO for Enhanced Corrosion Protection and Multifunctional Performance on Carbon Steel. Journal of Polymer & Composites. 2026; 14 (1): 216–238p.

Keywords: Superhydrophobic coating, Micro-CaCO3/ nano-ZnO, Mechanical robustness durability, wear/corrosion resistance

INTRODUCTION

Carbon steel is extensively employed in industries such as aerospace, construction, transportation, building, automotive and electronics owing to its superior mechanical properties and favorable strength-to-weight ratio [1,2]. However, its vulnerability to corrosion, friction, and adhesion remains a critical limitation, often resulting in diminished service efficiency, structural degradation, environmental hazards, resource wastage, and financial losses [3]. To overcome these challenges, numerous protective approaches have been investigated, including micro-arc oxidation [4], sacrificial anodes [5], organic coatings [6], and corrosion inhibitors [7]. Among these, protective coatings are particularly attractive due to their cost-effectiveness, ease of maintenance, and ability to simultaneously improve corrosion resistance and tribological performance.

In recent years, superhydrophobic coatings, which generate a composite solid–gas–liquid interface, have attracted significant interest. These coatings not only repel corrosive liquids but also suppress adhesion caused by capillary condensation [8]. Defined by a water contact angle (WCA) exceeding 150° and a sliding angle (SA) below 10°, such surfaces exhibit multifunctional properties, including anti-icing [9], corrosion resistance [10], friction reduction [11], and self-cleaning [12]. These features render them highly suitable for extending material durability under harsh conditions. The fabrication of superhydrophobic coatings typically involves two essential steps: engineering hierarchical surface roughness and lowering surface energy [13]. Various fabrication techniques have been reported, such as anodization [13], electrodeposition [14], femtosecond laser treatment [15], hydrothermal synthesis [16], chemical etching [17], spray coating [18], drilling technique [19] and sol–gel processing [20], since the first report of a superhydrophobic surface by Ollivier in 1907 [21].

Despite these advancements, superhydrophobic coatings frequently suffer from poor adhesion and fragile micro–nano surface structures that deteriorate under mechanical stresses such as friction and impact [22]. Consequently, the development of mechanically robust, self-healing, and anti-friction coatings has become a key research priority. Reinforcement strategies using micro- and nano-sized fillers (e.g., SiO_2, TiO_2, Al_2O_3, graphene oxide, Montmorillonite nanoclay, natural fibers) have shown promise in enhancing durability [23,24,25,26]. For instance, Yap et al. [27] fabricated a SiO_2 nanoparticle-based coating with improved mechanical integrity and self-cleaning ability, while Yang et al. [28] and Wang et al. [29] reported enhanced mechanochemical stability and reusability using hBN/Al_2O_3 and SiO_2/GO nanocomposites, respectively. Nevertheless, many existing strategies fail to adequately address the intrinsic stability of the micro–nano structures that underpin long-term performance.

To address this issue, a durable superhydrophobic coating was developed on carbon steel substrates via a simple and economical one-step brushing method. The coating was reinforced with micro-sized calcium carbonate ($CaCO_3$) and nano-sized zinc oxide (ZnO) particles to enhance its mechanical stability. ZnO was chosen for its high melting point (~1975 °C), flame retardancy, thermal conductivity, electrical resistivity [30], lubricating behavior [31], and modifiable surface properties, while $CaCO_3$ contributed to improved wear resistance and corrosion protection [25]. Accordingly, an EP/PDMS@micro-$CaCO_3$/nano-ZnO composite superhydrophobic coating was systematically designed and fabricated. The influence of varying $CaCO_3$ and ZnO content on wettability, microstructure, and surface morphology was examined, and its multifunctional performance—including anti-icing, buoyancy enhancement, self-cleaning, anti-fouling, thermal stability, tribological properties, corrosion resistance, and mechanical durability—was thoroughly evaluated. Overall, this study demonstrates a practical, scalable strategy for fabricating multifunctional superhydrophobic coatings with promising applications in environments demanding superior material protection.

EXPERIMENTAL SECTION

Materials and Reagents

Polydimethylsiloxane (PDMS) and its curing agent were procured from LabChem Sdn Bhd, Selangor, Malaysia. Bisphenol A diglycidyl ether (DGEBA) epoxy resin and its associated curing agent were

obtained from Sky Tech Malaysia Sdn Bhd, Selangor, Malaysia. Ethanol, sodium hydroxide (NaOH), hydrochloric acid (HCl), and acetone were supplied by Merck Millipore, Darmstadt, Germany. Micro-sized calcium carbonate ($CaCO_3$, 99.9% purity) with particle diameters ranging from 5 μm to 10 μm was sourced from Sigma Aldrich, Selangor, Malaysia. Nano-sized zinc oxide (ZnO, 99.99% purity) with an average particle size of approximately 20 nm was purchased from Fisher Scientific International Inc., India. Deionized water with a resistivity of approximately 15.0 MΩ was prepared using a Nanopores ultrapure water system. All chemicals and solvents were used as received without any further purification. S50C carbon steel (CS) sheets (Special Steel & Alliance Sdn Bhd) were used as substrates, cut into dimensions of 25 × 75 × 3 mm^3, with their chemical compositions listed in Table 1. GCr15 bearing steel balls with a diameter of 4.5 mm were employed as counterface materials in tribological testing.

Preparation of EP/PDMS@Micro-CaCO3/Nano-ZnO Coating

S50C carbon steel (CS) sheets were mechanically polished with silicon carbide abrasive papers up to 1000 grit, followed by ultrasonic cleaning in acetone to remove residual grease. After drying with compressed air, the substrates were preheated at 80 °C for 30 minutes in a laboratory oven to enhance coating adhesion. To optimize the micro-$CaCO_3$ content, different amounts (0.1–0.6 g) were dispersed in a mixture containing 0.60 g PDMS and 0.10 g EP dissolved in 10 mL ethanol. The suspension was magnetically stirred for 1 hour to ensure homogeneity. Subsequently, 0.05 g of EP curing agent and 0.05 g of PDMS curing agent were introduced into the solution and stirred for an additional 15 minutes. The resulting suspension was applied onto the substrate surface using a brushing technique, ensuring complete coverage. Coated samples were then cured at 100 °C for 45 minutes to promote strong adhesion. Following the optimization of $CaCO_3$ content, various amounts of nano-ZnO (0.05–0.35 g) were incorporated into the optimized $CaCO_3$-based suspension to investigate the synergistic effects of micro- and nano-fillers. A schematic illustration of the fabrication procedure for the superhydrophobic EP/PDMS@micro-$CaCO_3$/nano-ZnO coating is shown in Figure 1.

Table 1. Chemical composition of S50C CS

Elements	C	Si	S	Mn	P	Ni	Al	Fe
wt.%	0.150	0.180	0.031	0.450	0.010	0.008	0.005	99.166

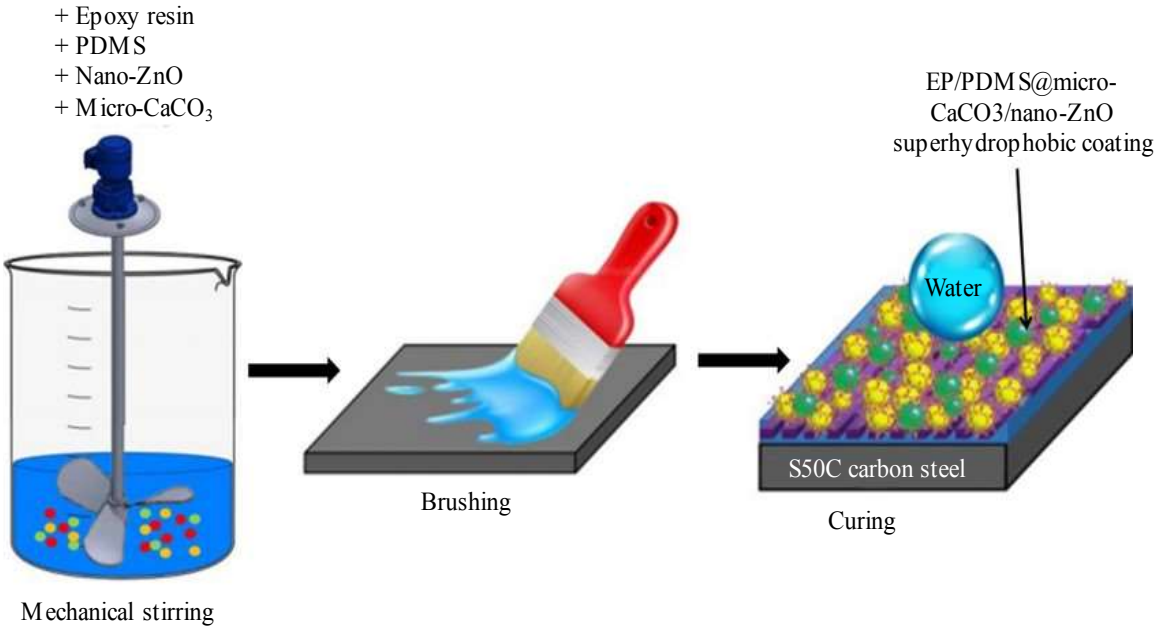

Figure 1. Fabrication procedure for the superhydrophobic EP/PDMS@micro-$CaCO_3$/nano-ZnO coating.

Characterizations

The static water contact angles (WCAs) and sliding angles (SAs) were measured using a contact angle goniometer (OCA 15EC Pro, Dataphysics, Filderstadt, Germany). Image analysis was conducted using ImageJ software (National Institutes of Health, USA) equipped with the Low Bond Axisymmetric Drop Shape Analysis (LBADSA) plugin. Deionized water droplets (10 μL) were used, and measurements were performed at seven different locations on each sample, with the average values reported to ensure data reliability. Surface morphology was examined by field emission scanning electron microscopy (FESEM, JSM-78000, JEOL, Tokyo, Japan) operated at a 5.0 kV accelerating voltage and 10 μA beam current. Elemental analysis was performed using energy-dispersive X-ray spectroscopy (EDS) attached to the FESEM Prior to imaging, samples were sputter-coated with a ~150 nm thick Platinum/Palladium layer using a JEC-3000FC Auto-Fine Sputter Coater under an 18 mA current to minimize surface charging. The three-dimensional surface topography and roughness were characterized using confocal laser scanning microscopy (CLSM, LEXT OLS4100, Olympus, Tokyo, Japan). X-ray photoelectron spectroscopy (XPS, ESCALAB 250Xi+, Thermo Fisher Scientific, UK) was employed to determine the surface elemental compositions.

Mechanical Stability

The mechanical robustness of the coatings was evaluated through a sandpaper abrasion test. Coated samples were placed on 2000-grit SiC sandpaper under a 300 g applied load and moved at a constant speed of 5 mm/s. Each abrasion cycle consisted of a 10 cm forward and 10 cm backward movement (total 20 cm). After each cycle, WCA and SA measurements were recorded to assess changes in wettability and determine the mechanical stability of the coatings.

Tribological Test

The tribological performance of the coatings was evaluated using a UMT Multi-Specimen Test System (UMT5, Bruker, USA) in a ball-on-disk configuration. A cleaned GCr15 steel ball (diameter 4.5 mm) served as the counterface, while the coated samples acted as the disk. Tests were conducted under a reciprocating sliding motion with a stroke length of 6 mm per pass. The sliding velocity, ambient temperature, Hertzian contact pressure, relative humidity, and total test duration were set at 1 mm/s, 26 °C, 500 N/mm², 35%, and 1800 s, respectively. The coefficient of friction was continuously recorded by a computer linked to the UMT system. Each test was repeated five times to ensure statistical reliability and reproducibility of the results.

Electrochemical Tests

The corrosion resistance of the samples was assessed using an electrochemical workstation (CS312M, CorrTest, China) in a 3.5 wt% NaCl aqueous solution. The working electrode was the sample (1 cm² exposed area), with a platinum mesh (20 mm × 20 mm) serving as the counter electrode and a saturated calomel electrode (SCE) as the reference electrode. Electrochemical impedance spectroscopy (EIS) was conducted after stabilizing the open circuit potential (OCP), using a 10 mV sinusoidal perturbation in the frequency range of 100 kHz to 0.01 Hz. Potentiodynamic polarization (PDP) measurements were carried out by scanning the potential from −0.3 $V_{\_SCE}$ to 0.3 $V_{\_SCE}$ at a sweep rate of 0.2 mV/s. Corrosion parameters, including corrosion current density (Icorr) and corrosion potential (Ecorr), were determined using Corroview software by extrapolating the linear portion of the polarization curve.

Evaluation of Multifunctional Properties

The multifunctional properties of the superhydrophobic coating were systematically evaluated under different practical conditions, including self-cleaning, anti-fouling, anti-icing, thermostability, and buoyancy enhancement. The tests were conducted as follows: (1) Self-cleaning: Standard sands were applied to the coating surface, followed by water droplets to observe the removal of contaminants, indicating the self-cleaning behavior. (2) Anti-fouling: The sample was submerged in common liquids such as slurry, coke, milk, and tea, and any residue of liquid or solid contaminants was checked after

removal. (3) Anti-icing: Coated and uncoated samples with water droplets were placed in a refrigerator at −10 °C for 10 minutes, and the freezing behavior of the droplets was observed through macrographs taken every 40 seconds. (4) Thermal stability: Coated samples were heated at 100 °C, 300 °C, 500 °C, 700 °C, and 900 °C for 10 minutes and subsequently cooled to room temperature. Water droplets were applied to evaluate the water repellency at each temperature. (5) Buoyancy enhancement: Samples were placed on water to test their buoyancy. A balance was maintained by adjusting weights placed on a glass slide to determine the maximum load the sample could carry. (6) Substrate Versatility Test: The coating's water repellency was further tested on substrates with varying physical and chemical properties, such as glass slides, abrasive paper, plastics, fabrics, and wood.

RESULTS AND DISCUSSION

Wettability and Surface Morphology of Coating

Figure 2 illustrates the variation in water contact angles (WCAs) and sliding angles (SAs) of the bare S50C carbon steel substrate and EP/PDMS@micro-$CaCO_3$ composite coatings with different amounts of micro-$CaCO_3$ incorporation. The bare S50C surface exhibited an initial WCA of 80.5°± 1.9°, characteristic of its inherent hydrophilic nature. Upon coating with EP/PDMS (without any micro-$CaCO_3$ addition), the surface wettability transitioned to hydrophobicity, with the WCA increasing to 109.3°± 2.5°. With the incorporation of various masses of micro-$CaCO_3$ specifically 0.1 g, 0.2 g, 0.3 g, 0.4 g, 0.5 g, and 0.6 g, the WCA values of the corresponding coatings were observed to be 145.1°± 5.3°,157.6°± 1.7°,158.8°± 4.1°,153.6°± 6.2°,151.4°± 3.6°, and 144.37°± 5.5°. respectively. In parallel, the SAs for the samples with 0.4 g, 0.5 g, and 0.6 g micro-$CaCO_3$ additions were measured at 2.7°± 1.2°, 2.8°± 3.7° and 3.77°± 4.5°, respectively.

These findings demonstrate that the addition of 0.4 g micro-$CaCO_3$ yields an optimal balance between achieving a high WCA and maintaining a relatively low SA. Specifically, the coating with 0.4 g micro-$CaCO_3$ exhibits a superhydrophobic behavior, characterized by a WCA close to 160° and a low sliding angle, suggesting enhanced water-repellency and reduced liquid adhesion. This optimal performance is attributed to the synergistic effects of surface chemistry modification and micro/nanostructured roughness introduced by micro-$CaCO_3$ fillers within the EP/PDMS matrix.

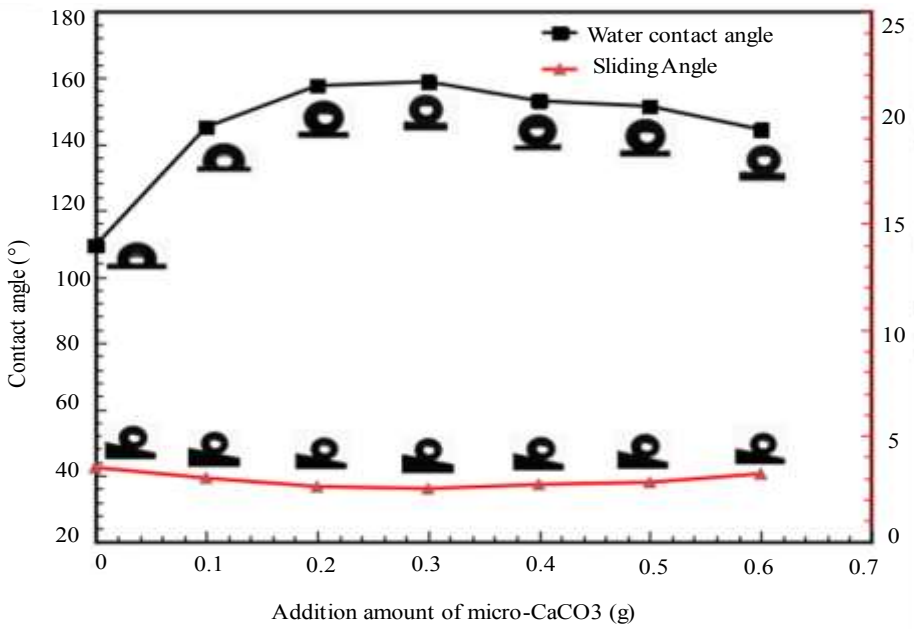

Figure 2. The variation in water contact angle (WCAs) and sliding angle (SAs) of bare S50C carbon steel substrate and EP/PDMS@micro-$CaCO_3$ composite coating with different amounts of micro-$CaCO_3$ incorporation.

In summary, the water contact angle (WCA) on the coating surface increases progressively with the rising content of micro-$CaCO_3$ particles. The highest hydrophobicity was achieved with the addition of 0.4 g of micro-$CaCO_3$, resulting in a WCA of 158.8°± 4.1° and a sliding angle (SA) of 13.3∘±0.9. However, further increases in micro-$CaCO_3$ content, beyond 0.4 g, lead to a decrease in the WCA. This decline can be attributed to the agglomeration of micro-$CaCO_3$ particles at higher concentrations. The excessive particle loading reduces the porosity of the coating, consequently diminishing the volume of air trapped within the surface. This reduction in the trapped air volume lowers the water repellency, leading to a decline in the WCA and, thus, a decrease in hydrophobic performance.

The optimal addition of micro-$CaCO_3$ to the coating is found to be 0.4 g, under which the superhydrophobic properties are maximized. The uniform application of PDMS, EP, micro-$CaCO_3$ particles, ethanol, PDMS curing agent, and EP curing agent on the S50C CS surface contributes to the enhancement of the coating's roughness. The micro-$CaCO_3$ particles are effectively encapsulated within the PDMS matrix and bonded with the EP resin, forming a durable and structured composite on the S50C CS surface. This structure provides the requisite roughness to facilitate the formation of an air cushion, which aids in repelling liquids and mitigating corrosion. Moreover, the sliding angle of the EP/PDMS@micro-$CaCO_3$ coating remains above 5°, classifying it as a low-adhesion superhydrophobic surface, which may benefits its potential applications where ultra-low sliding angles are required.

To further enhance the adhesion resistance of the coating, nano-ZnO was incorporated into the previously described suspension to form a EP/PDMS@micro-$CaCO_3$/nano ZnO coating. Initially, with 0.4 g of micro-$CaCO_3$, the addition of nanoZnO resulted in an excessively thick suspension, making it difficult to apply the coating evenly during brushing. Consequently, the amount of micro-$CaCO_3$ was maintaned and the nano ZnO content was adjusted to identify the optimal formulation. Figure 3 illustrates the variation of water contact angles (WCAs) and sliding angles (SAs) for the coated samples with increasing amounts of nano ZnO.

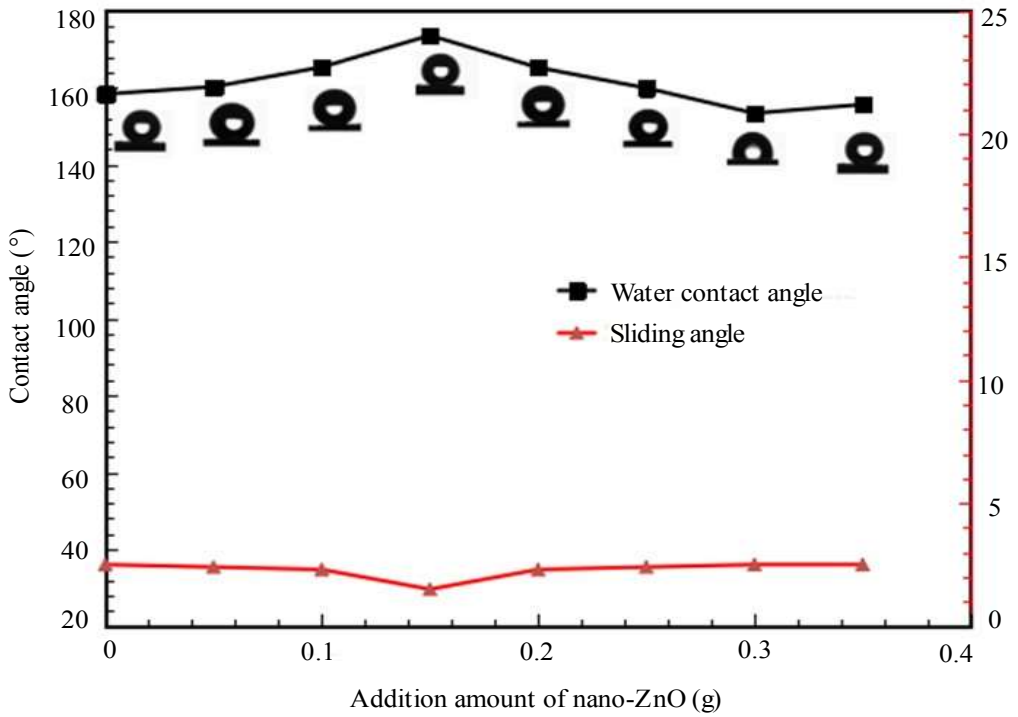

Figure 3. WCAs and SAs of EP/PDMS@micro-$CaCO_3$ /nano-ZnO coating with different nano-ZnO additions.

The WCAs exhibited an increasing trend when nano-ZnO content was below 0.15 g, but declined once the amount surpassed this threshold. Conversely, the SA displayed a reverse trend. The sample containing 0.40 g of micro-$CaCO_3$ and 0.15 g of nano-ZnO, referred to as the 0.40 $CaCO_3$ -0.15ZnO samples$_3$ sample, showed a WCA of 173.54° ± 2.53° and an SA of 1.5° ± 1.12°, indicative of superhydrophobicity. This enhancement in performance can be attributed to the contribution of micro-$CaCO_3$ and nano-ZnOin creating micro- and nano-scale structures, which form a hierarchical micro/nanostructure. Additionally, the modification of the surface with PDMS further reduces the surface energy, contributing to the superhydrophobic behavior. Higher filler content generally decreased dimensional consistency and impact strength but increased stiffness [32]

The filler loadings used in this study were optimized through a systematic experimental approach. Preliminary trials were conducted by varying the Micro-$CaCO_3$ and Nano-ZnO contents within the EP/PDMS matrix. The optimal formulation was selected based on a balance of superhydrophobicity, coating adhesion, mechanical integrity, and corrosion resistance. Excessive filler loading was found to adversely affect coating uniformity and mechanical stability, while insufficient loading resulted in reduced surface roughness and barrier performance. The selected filler concentrations therefore represent the optimal compromise to achieve multifunctional performance.

To further characterize the distribution of nano-ZnO, high-magnification Field Emission scanning electron microscopy (FESEM) images of the (a)EP/PDMS coating (b) 0.4g micro-$CaCO_3$ and (c)0.40 $CaCO_3$ -0.15ZnO samples were captured, as shown in Figure 4. These images reveal that the nano-ZnO nanoparticles are primarily distributed on the surface of the $CaCO_3$ particles, suggesting that the moderate amount of nanoparticles in the suspension prevents the formation of severe agglomerates, contributing to the uniformity and effectiveness of the coating. It is evident that nano-ZnO particles are interspersed between the gaps and on the surface of micro-$CaCO_3$, facilitating the formation of a binary hierarchical micro-nano structure. When the addition of nano-ZnO is less than 0.15 g, the lack of sufficient nanoscale structure to support the water droplets leads to lower WCAs and higher SAs. However, when the amount of nano-ZnO exceeds 0.15 g, particle aggregation occurs, resulting in a non-uniform coating that leads to a significant decrease in WCA and an increase in SA.

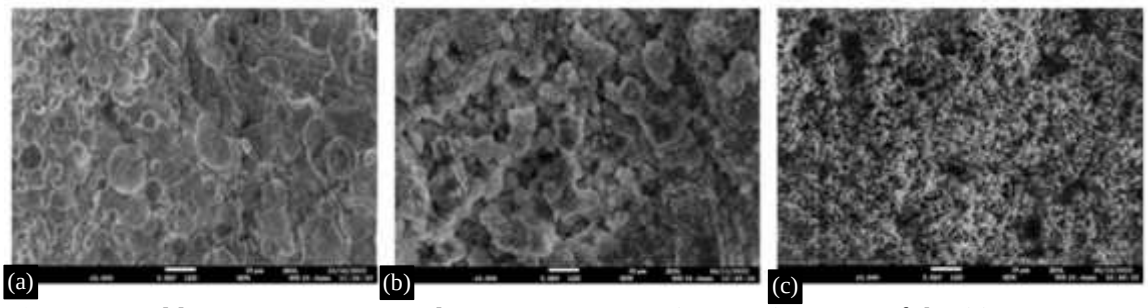

Figure 4. Field Emission scanning electron microscopy (FESEM) images of the (a)EP/PDMS coating (b) 0.4g micro-$CaCO_3$ and (c) 0.40 $CaCO_3$ -0.15ZnO samples.

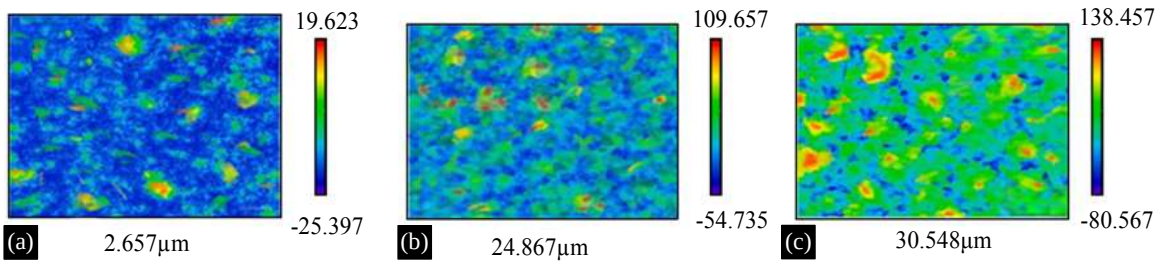

Figure 5. Surface roughness images of the (a)EP/PDMS coating (b) 0.4g micro-$CaCO_3$ and (c) 0.40 $CaCO_3$ -0.15ZnO samples.

Wettability is strongly influenced by surface roughness, which plays a key role in determining the hydrophobic or hydrophilic properties of a surface. The surface roughness of coatings with varying amounts of micro-$CaCO_3$ addition was evaluated using Confocal Laser Scanning Microscopy (CLSM). For the bare S50C CS sample, the surface is relatively flat and smooth, exhibiting a low average surface roughness (Sa) of 0.234 μm. Upon applying a mixture of PDMS, PDMS curing agent, EP, EP curing agent, and ethanol without the inclusion of any microparticles, the Sa value increased significantly to 2.657 μm (Figure 5a).

With the incorporation of micro-$CaCO_3$ into the brushing solution, the surface roughness further increased. A marked change occurs when the addition of micro-hBN exceeds 0.4g. As seen in Figure 4b, the surface roughness experiences a significant jump to 24.867 μm with the addition of 0.4 g of micro-$CaCO_3$. Beyond this point, further increases in micro-$CaCO_3$ content result in only a slight increase in surface roughness This abrupt increase in roughness can be attributed to the formation of a more pronounced hierarchical structure on the coating surface as the micro-$CaCO_3$ content rises, which may further enhance the coating's hydrophobic characteristics.The addition of nano-ZnO increased the surface roughness to 30.548μm where it remarks high superhydrophobicity.

Therefore, the optimal addition of micro-$CaCO_3$ and nano-ZnO is determined to be 0.40 g and 0.15 g, respectively. Under these conditions, the coating achieves a WCA of 173.54° ± 2.53° and an SA of 1.5° ± 1.12°. The micro-nano hierarchical structure provides adequate roughness, creating large air gaps and an air cushion that repels liquid and reduces the likelihood of corrosion reactions. This behavior aligns with the Cassie-Baxter non-wetting model, where the air cushion formed within the micro-nano structure significantly decreases the solid-liquid contact area while increasing the liquid-air contact area, thus promoting superhydrophobicity.

The superior performance of the EP/PDMS coating incorporating the hybrid Micro-$CaCO_3$/Nano-ZnO filler system can be attributed to the synergistic interaction between micro- and nano-scale fillers. Micro-$CaCO_3$ particles contribute to the development of hierarchical surface roughness and enhance mechanical integrity by acting as stress-bearing reinforcements within the polymer matrix. Meanwhile, Nano-ZnO particles effectively fill micro-voids and defects, leading to improved coating compactness and barrier properties. In addition, the presence of ZnO nanoparticles promotes enhanced corrosion resistance due to their chemical stability and ability to hinder electrolyte penetration. Compared to single-filler or binary systems reported in recent literature, the combined micro-nano filler configuration in this study provides a more continuous tortuous diffusion pathway for corrosive species, resulting in higher water contact angles, improved durability, and superior corrosion protection performance.

Chemical Compositions of Coating

Energy-dispersive X-ray spectroscopy (EDS) is widely used to characterize the elemental composition of coating surfaces [26]. Quantitative EDS analysis of the 0.40 $CaCO_3$ -0.15ZnO sample reveals that the superhydrophobic coating comprises Ca, Si, Zn, C, and O, with mass fractions of 12.8%, 18.1%, 9.6%, 25.3%, and 29.6%, respectively, and atomic fractions of 3.4%, 6.8%, 1.6%, 22.2%, and 19.5% respectively. These findings suggest that low-surface-energy polydimethylsiloxane (PDMS) and and micro-$CaCO_3$ /nano-ZnOparticles adhere and bond effectively to the s50C CS substrate.

To further elucidate the surface chemical characteristics, X-ray photoelectron spectroscopy (XPS) was conducted. The full survey spectrum identifies C 1s, O 1s, , Si 2p, Ca 2p, and ZnO signals. The elements C, Si, and O detected are primarily derived from PDMS. During magnetic stirring, ZnO and $CaCO_3$ particles are thoroughly modified by long-chain PDMS molecules, imparting strong hydrophobicity. In a polar medium, the PDMS coating protects the residual hydroxyl groups on the $CaCO_3$ and ZnO surfaces, preventing excessive wetting. The combination of residual hydroxyl groups and hydrophobic chains leads to the formation of stable hydrophobic particles.
Thus, EDS and XPS results collectively confirm that PDMS successfully modifies micro-$CaCO_3$ and nano-ZnO particles, effectively reducing the surface energy and facilitating the construction of a durable superhydrophobic coating on S50C Carbon steel Substrate.

Mechanical Durability

In superhydrophobic materials, the micro/nano-scale hierarchical surface structures are highly susceptible to mechanical damage when exposed to external forces. Consequently, the mechanical robustness of artificial superhydrophobic coatings remains a critical challenge that significantly restricts their broader practical applications. To address this issue, a sandpaper abrasion test was employed to systematically evaluate the abrasion resistance of the developed coating [27]. The schematic representation of the abrasion testing setup and the corresponding experimental results are presented in Fig. 6a and b. Remarkably, after undergoing a total abrasion distance of 400 cm against 2000-grit sandpaper, the coating maintained a high water contact angle (WCA) of 153.90° ± 2.25° and a sliding angle (SA) of 3.56° ± 0.60°, with only a minimal change in wettability. These results clearly indicate that the coating exhibits outstanding abrasion resistance.

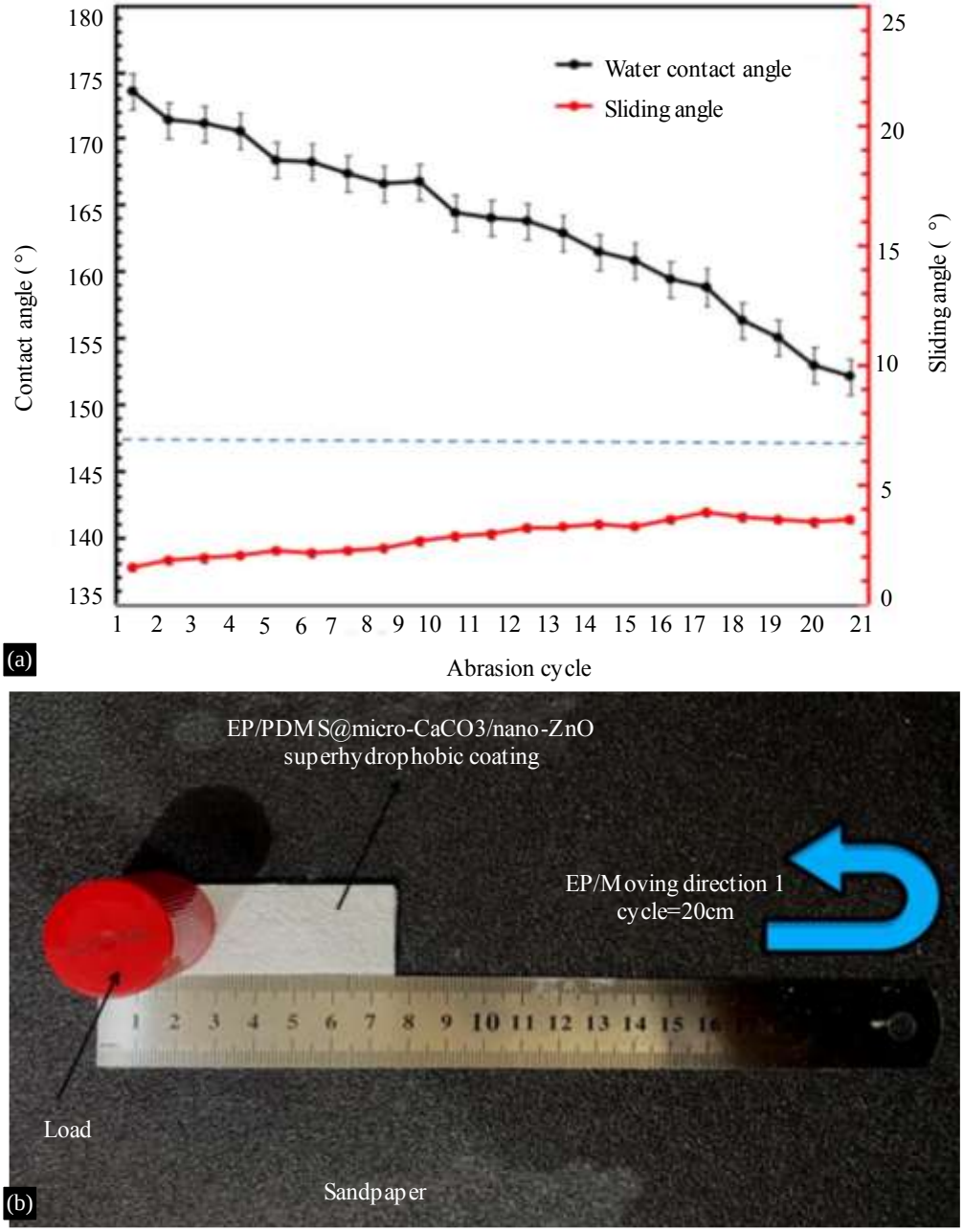

Figure 6. The schematic representation of the abrasion testing setup and corresponding experimental results for the test.

This robust mechanical performance can be attributed to two primary factors. Firstly, the incorporation of resin within the EP/PDMS@micro-$CaCO_3$/nano-ZnO composite structure significantly enhances cohesion among the PDMS@micro-$CaCO_3$/nano-ZnO constituents. The formation of a dense, crosslinked network between the resin matrix and the micro/nanoparticles, along with the secure embedding of these particles within the surface layer, substantially reinforces the mechanical durability of the coating. Secondly, the unique three-dimensional wurtzite crystal network structure of ZnO, which inherently possesses excellent lubricating properties, contributes further to the coating's wear resistance. The synergistic effect of these factors ensures that the coating retains its superhydrophobic characteristics even after extensive mechanical wear.

Although cyclic mechanical loading or bending tests were not explicitly conducted in this study, the coating's mechanical robustness can be inferred from the abrasion resistance and adhesion performance results. The incorporation of PDMS imparts inherent flexibility to the coating, enabling effective stress dissipation under mechanical deformation. Furthermore, Micro-$CaCO_3$ particles enhance load-bearing capacity, while Nano-ZnO particles improve interfacial bonding within the polymer matrix. Similar EP/PDMS-based composite coatings have been reported in the literature to exhibit stable performance under repeated bending and cyclic loading conditions, suggesting that the developed coating possesses promising mechanical durability for practical applications.

Tribological Performance

The micro-friction behavior of bare S50C carbon steel (CS) and the EP/PDMS@micro-$CaCO_3$/nano-ZnO coated surface was investigated under controlled conditions (Hertz contact pressure: 500 N/mm; duration: 1800 s; sliding velocity: 1 mm/s), with both samples tested against a GCr15 steel ball. The friction coefficient profiles are presented in Figure 7. As illustrated, the friction coefficient of the uncoated S50C CS surface exhibited a rapid increase, reaching approximately 1.30 within the initial 25 seconds of sliding. In sharp contrast, the EP/PDMS@micro-$CaCO_3$/nano-ZnO coated surface maintained a low and stable friction coefficient of around 0.31 throughout the entire test duration. To quantify the tribological improvement, the efficiency of friction coefficient reduction (η) was calculated using the following equation [33]:

$$\mu = \frac{(f_{bare} - f_{shb}) \times 100\,\%}{f_{bare}} \quad (1)$$

where f_{bare} represents the friction coefficient of the bare S50C CS surface, and f_{shb} denotes that of the superhydrophobic coated surface. Based on this formula, the coating achieved a friction reduction efficiency of 76.2%.

The significantly enhanced tribological performance of the coated surface can be attributed to several synergistic factors. Firstly, the intrinsically low surface energy of the EP/PDMS@micro-$CaCO_3$/nano-ZnO composite contributes to reduced interfacial adhesion during sliding. Secondly, the ZnO nanoparticles embedded within the coating impart a lubricating effect that facilitates smoother sliding. Additionally, the strong bonding between the resin matrix and the micro/nanoparticles ensures mechanical integrity under stress. Finally, the presence of protruding ZnO and $CaCO_3$ particles provides an antiwear effect, collectively ensuring sustained low friction and superior wear resistance.

Corrosion Resistance Evaluation

In this study, the corrosion behavior was evaluated through electrochemical analysis based on fitted parameters and the morphology of impedance curves. Electrochemical impedance spectroscopy (EIS) measurements were performed on both bare S50C carbon steel (CS) and the EP/PDMS@micro-$CaCO_3$/nano-ZnO coated samples (specifically, 0.40$CaCO_3$ -0.15ZnO) to assess their corrosion resistance. As shown in Figure 8a, the Nyquist plots reveal that the capacitive arc radius for the coated sample is significantly larger than that of the bare substrate, indicating an enhanced anti-corrosion performance imparted by the coating.

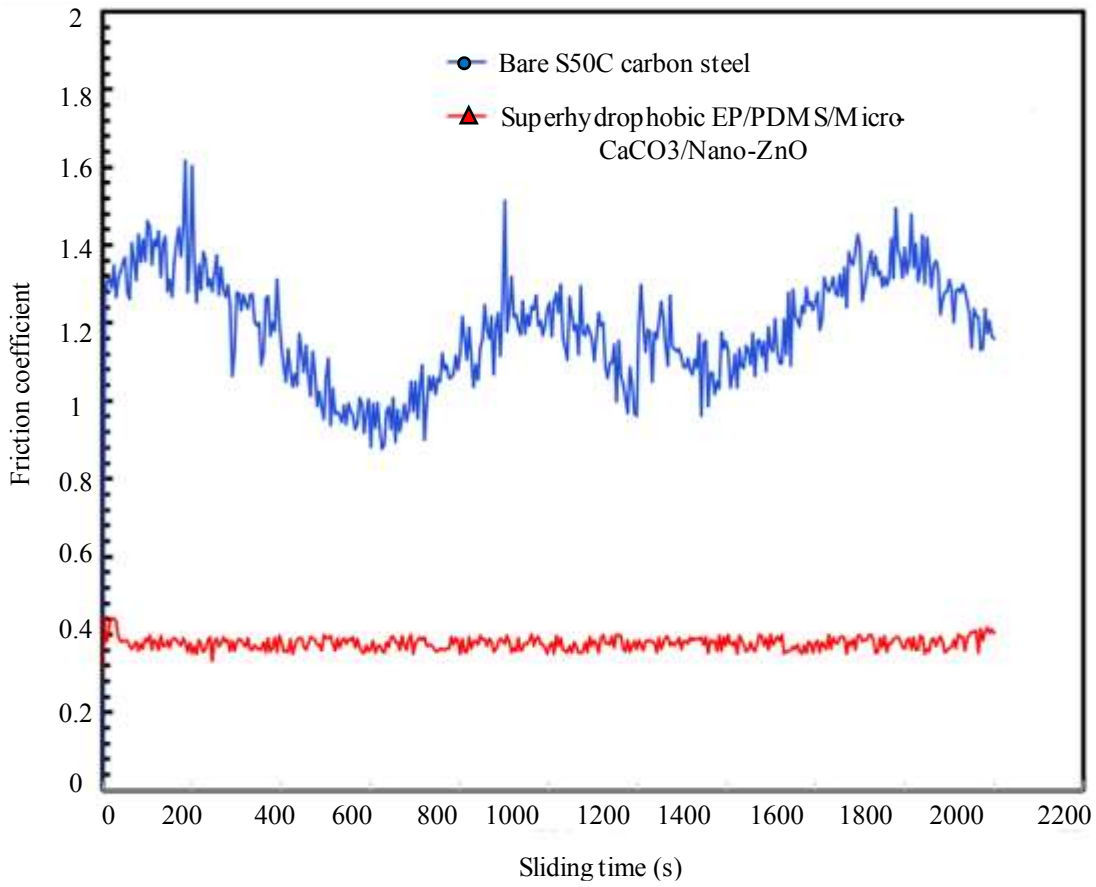

Figure 7. Friction coefficient profiles.

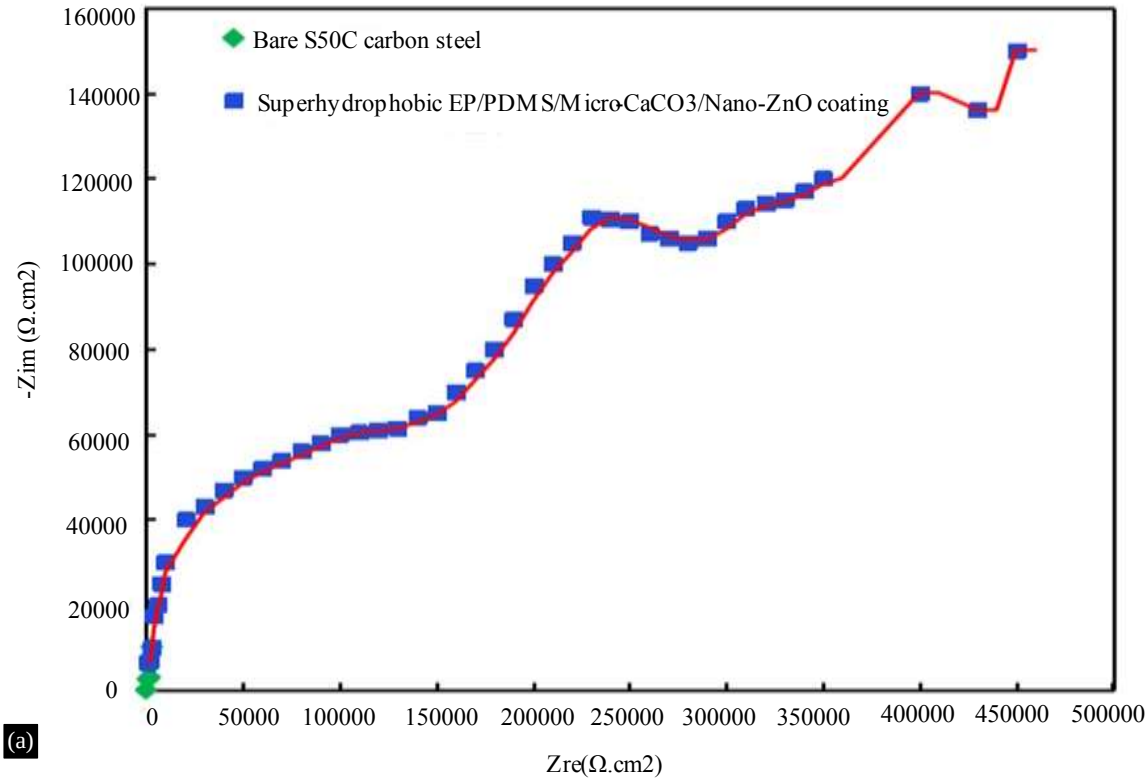

(a)

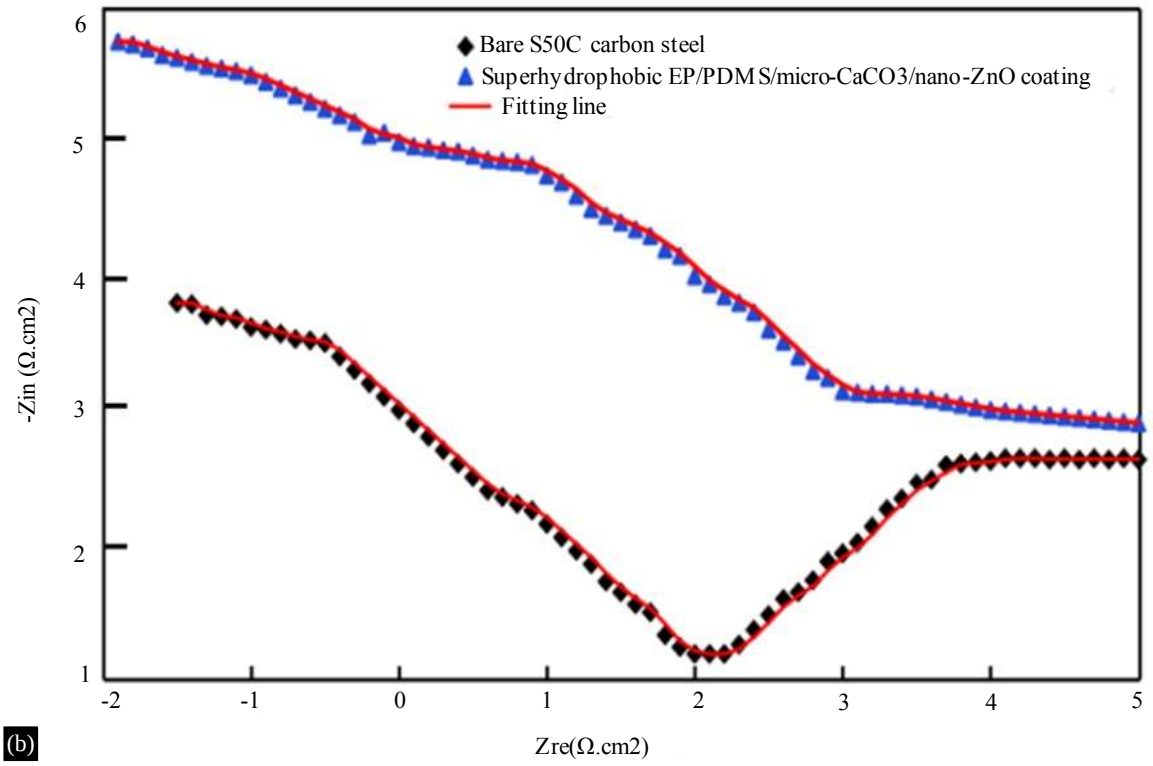

Figure 8. (a) Nyquist plots, (b) Bode plots of log |Z| vs. log f of bare S50C CS and 0.40$CaCO_3$ -0.15ZnO samples.

Conventionally, the impedance modulus ($|Z|_{0.01\ Hz}$) at low frequency serves as a key indicator of the corrosion resistance capabilities of protective coatings. Fig. 8b presents the Bode plots of log|Z| versus log f for both the bare and coated samples. The ($|Z|_{0.01\ Hz}$) value for the coated sample was recorded at $4.8\times10^5\ \Omega cm^2$, which is approximately two orders of magnitude greater than that of the bare S50C CS ($6.4\times10^3\ \Omega cm^2$. The larger capacitive arc and the elevated low-frequency impedance collectively demonstrate that the EP/PDMS@micro-$CaCO_3$/nano-ZnO coating substantially improves corrosion resistance.

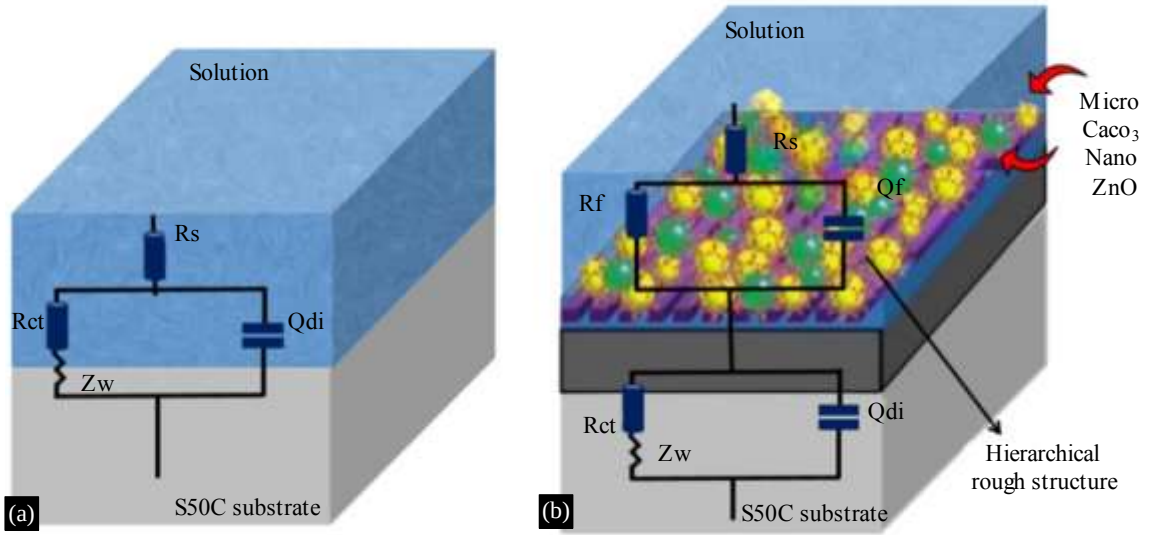

Figure 9. Electrochemical equivalent circuits of (a) bare S50C CS and b) 0.40 $CaCO_3$ -0.15ZnO samples.

For a more detailed electrochemical comparison, the EIS data were fitted using equivalent circuit models, specifically R(Z(Q)) for the bare S50C CS and R(QR)(RZ(Q)) for the coated samples, as depicted in Figure 9a and 9b, respectively. In these models, R_s, R_{ct}, and R_f represent the solution resistance, charge transfer resistance, and coating resistance, respectively. Q_f and Q_{dl} denote the capacitances associated with the coating/solution interface and the substrate/solution double layer, respectively. Additionally, Warburg impedance (Z_W) was included to account for ion diffusion effects at very low frequencies.

The corresponding fitted parameters are listed in Table 2. Notably, the coated sample exhibits a charge transfer resistance (R_{ct}) of $5.3\times10^5\ \Omega cm^2$, markedly higher than that of the bare sample ($2.5\times10^3\ \Omega cm^2$. The protection efficiency (P.E.%) of the coating was calculated using the formula [34]:

$$PE\% = (1\_\frac{R_{ct}^o}{R_{ct}^c}) \text{ x } 100 \quad (2)$$

Where and represent the charge transfer resistance of the bare substrate and the coated sample, respectively. The coating achieved a protection efficiency of 99.78%, confirming its effectiveness in shielding the substrate from corrosion.

To further validate the corrosion resistance, potentiodynamic polarization tests were conducted. Fig. 10a illustrates the polarization curves fitted via the Tafel extrapolation method, with detailed fitting parameters presented in Table 3. After immersion in a 3.5 wt% NaCl solution for 0.5 hours, the bare S50C CS exhibited a corrosion current density (I_{corr}) of 2.59×10^{-7} A/cm^2 and a corrosion potential (E_{corr}) of −0.67 V. In comparison, the coated sample showed a significantly reduced I_{corr} of 5.35×10^{-10} A/cm^2 and a positively shifted E_{corr} of −0.54 V. The protection efficiency (P.E.%) based on corrosion current densities was calculated using [29]:

$$PE\% = (1\_\frac{R_{ct}^o}{R_{ct}^c}) \text{ x } 100 \quad (3)$$

Table 2. Electrochemical parameters for EIS plots for bare S50C CS and 0.40 $CaCO_3$ -0.15ZnO samples.

Parameters	**Bare S50CS sample**	**0.40 $CaCO_3$ -0.15ZnO**
R_S (Ωcm^2)	32.35	35.78
R_{ct} (Ωcm^2)	2.5 x 10^3	5.3 x 10^5
R_f (Ωcm^2)	-	6.8 x 10^4
Q_f ($\Omega^{-1}cm^{-2}\ S^{n1}$)	-	2.4 x 10^{-7}
n_1(phase shift)	-	1.13
Q_{dl} ($\Omega^{-1}cm^{-2}\ S^{n2}$)	7.9 x 10^{-5}	3.5 x 10^{-6}
n_2 (phase shift)	0.99	0.54
Z_{W-R}	1.3 x 10^4	2.7 x 10^6
Z_{W-T}	23.1	399.4
β(Warburg coefficient)	0.56	0.97
PE%	-	99.78

Table 3. Dynamic potential polarization parameters of bare S50C CS and 0.40 $CaCO_3$ -0.15ZnO samples.

Parameters	**Bare S50CS sample**	**0.40 $CaCO_3$ -0.15ZnO**
E_{corr} (V)	-0.67	-0.54
I_{corr} (Acm^{-2})	2.59 x 10^{-7}	5.35 x 10^{-10}
PE %	-	99.90

where and are the corrosion current densities of the bare and coated samples, respectively. The EP/PDMS@micro-$CaCO_3$/nano-ZnO coated sample demonstrated an exceptional protection efficiency of 99.85%. This outstanding corrosion resistance is attributed to two primary factors: (1) the physically inert ZnO and $CaCO_3$ nanoparticles forming an effective barrier against aggressive ions and (2) the strong water repellency of the superhydrophobic coating, which traps an air cushion at the interface, significantly reducing the contact area between the corrosive solution and the substrate, as depicted in Figure 10b. Furthermore, the positive shift in E_{corr} suggests a lower corrosion tendency for the coated surface.

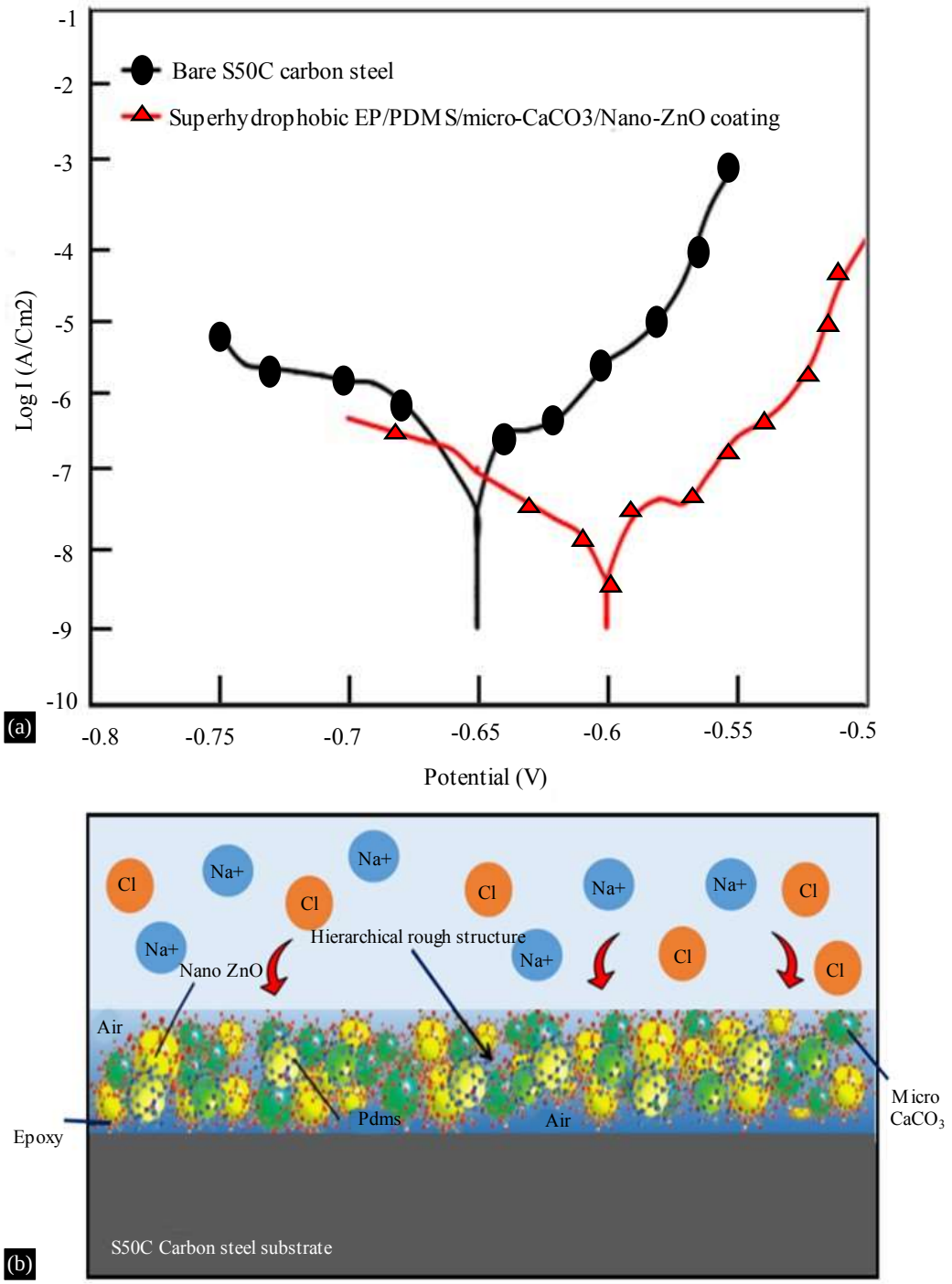

Figure 10. (a) Dynamic potential polarization curves of bare S50C CS and 0.40 $CaCO_3$ -0.15ZnO samples (b) Corrosion mechanism diagram of as-prepared superhydrophobic coating.

Comparative analysis with previous studies indicates that the EP/PDMS@micro-$CaCO_3$/nano-ZnO composite coating exhibits outstanding superhydrophobic characteristics that significantly hinder the infiltration of corrosive media, offering a promising solution for long-term corrosion protection in harsh environments.

Multi-Functionalities Performance

Self Cleaning Test

In practical applications, surfaces are unavoidably exposed to contamination by both solid particles and liquid pollutants, which can significantly compromise their appearance and functional performance. Therefore, developing surfaces with excellent self-cleaning and anti-fouling capabilities is of critical importance for maintaining their long-term reliability and aesthetic qualities.

To evaluate these properties, a self-cleaning test was conducted by uniformly sprinkling standard sand onto both bare S50C CS substrates and EP/PDMS@micro-$CaCO_3$/nano-ZnO-coated samples (0.40 CaCO3 -0.15ZnO formulation), as shown in Fig. 11a and 11b. The samples were positioned on a wooden platform inclined at a slope of 5°. Subsequently, dyed water droplets were dropped sequentially onto the upper edge of each sample to simulate rainfall washing. As illustrated in Fig. 11a, both the sand particles and the water droplets remained adhered to the bare S50C CS surface, indicating strong wetting and poor self-cleaning performance. In contrast, on the coated surface (Fig. 11b), the sand contaminants were rapidly and effectively removed by the flowing water droplets, without any residue remaining. These results clearly demonstrate that the fabricated superhydrophobic EP/PDMS@micro-$CaCO_3$/nano-ZnO coating endows the substrate with excellent water repellency and efficient self-cleaning behavior. The superior performance is attributed to the hierarchical surface texture and the stable air barrier formed at the solid–liquid interface, which minimize the adhesion between the contaminants and the surface.

Anti Fouling Test

Metallic surfaces, owing to their inherently hydrophilic nature and strong solid–liquid interfacial adhesion, are highly susceptible to contamination by liquid pollutants. In this study, the anti-fouling capability of the superhydrophobic 0.40 CaCO3 -0.15ZnO coated sample was systematically assessed using four common daily liquids—slurry, tea, coke, and milk as fouling media. The coated specimens were vertically immersed in each liquid, maintained for a defined period, and subsequently withdrawn. Each test was repeated five times to ensure the reliability and reproducibility of the results. As illustrated in Figure 12 the superhydrophobic coated samples exhibited excellent resistance to fouling, with no visible liquid residue adhering to their surfaces after immersion. In stark contrast, the bare S50C CS surfaces showed significant retention of contaminants, confirming their vulnerability to liquid fouling.

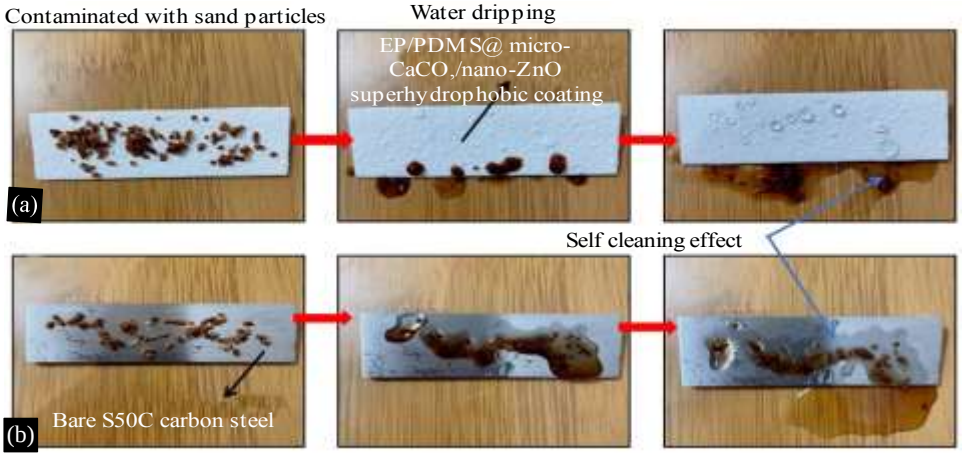

Figure 11. A Self-cleaning test was conducted by uniformly sparkling standard sand onto both (a) bare S50C CS subtrates and (b) EP/PDMS@micro-$CaCO_3$/nano-ZnO-coated samples (0.40 $CaCO_3$ - 0.15ZnO formulation)

The outstanding anti-fouling behavior of the superhydrophobic coating is primarily attributed to its ultra-low surface energy and hierarchical micro/nanostructure, which together create a stable air barrier at the interface. This trapped air layer minimizes the actual contact area between the solid and liquid phases, dramatically reducing adhesion forces and enabling liquids to easily roll off the surface without residue. Consequently, the superhydrophobic coating not only imparts superior self-cleaning performance but also effectively protects the underlying metallic substrate from corrosive media. In comparison, the uncoated S50C CS samples suffered extensive fouling, leading to surface degradation and potential compromise of their corrosion resistance. These findings highlight the critical role of surface engineering in enhancing the durability and functional lifespan of metallic materials in contaminated environments.

Furthermore, the mechanical robustness and stability of the superhydrophobic surface were further validated through high-pressure water splash tests. As depicted in Figure 13, water droplets rebounded from the coated surface without leaving any residual traces or signs of liquid infiltration. This behavior indicates the excellent integrity and durability of the micro/nanostructured surface layer under dynamic liquid impact.The resilience of the hierarchical surface textures, combined with the stable air layer trapped at the solid–liquid interface, are recognized as the primary contributors to the sustained superhydrophobic behavior. The fixed micro/nanostructures effectively minimize contact between the surface and impinging water, thereby maintaining a Cassie–Baxter wetting state even under mechanical perturbation. Collectively, these observations affirm that the EP/PDMS@micro-$CaCO_3$/nano-ZnO coating exhibits superior liquid repellency, robust self-cleaning capability, and durable antifouling performance. Such properties are critical for real-world applications where materials are frequently exposed to aggressive liquid environments and mechanical stresses.

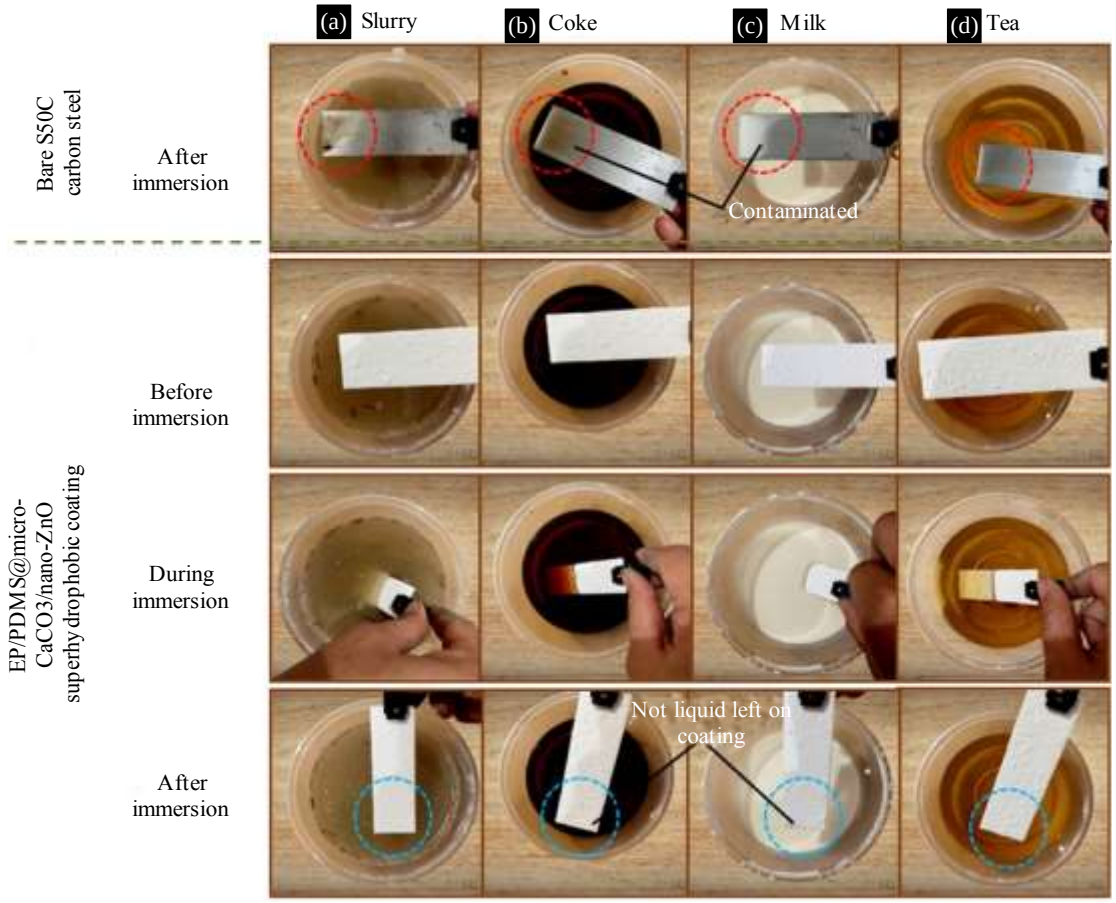

Figure 12. Anti-fouling capability of superhydrophobic 0.40 $CaCO_3$ -0.15ZnO coated samples was systematically assessed using four common daily liquids (a) slurry, (b) coke, (c) milk and (d) tea as fouling media

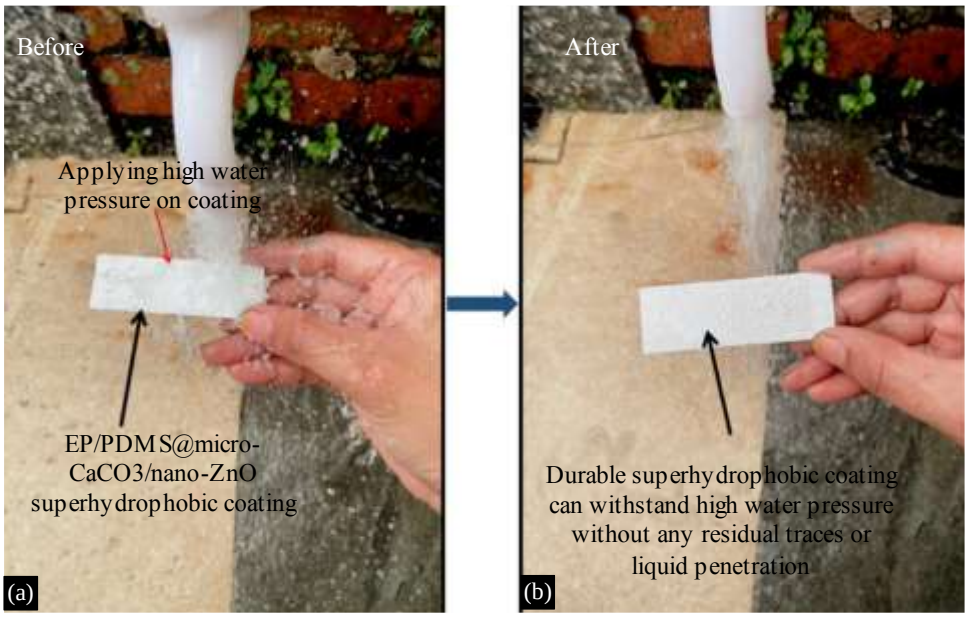

Figure 13. Water droplet rebounded from the coated surfaces without leaving any residual traces or signs of liquid infiltration.

Anti icing

In practical applications, materials inevitably encounter low-temperature environments, necessitating robust anti-icing properties. To assess this, the anti-icing behavior of the superhydrophobic EP/PDMS@micro-$CaCO_3$/nano-ZnO coated S50C carbon steel (CS) surface was systematically compared with that of the uncoated S50C CS. Two droplets of deionized water were carefully placed on the surfaces of both specimens, which were then transferred to a refrigeration chamber maintained at −10 °C. Sequential images were captured at 40-second intervals to monitor the freezing process.

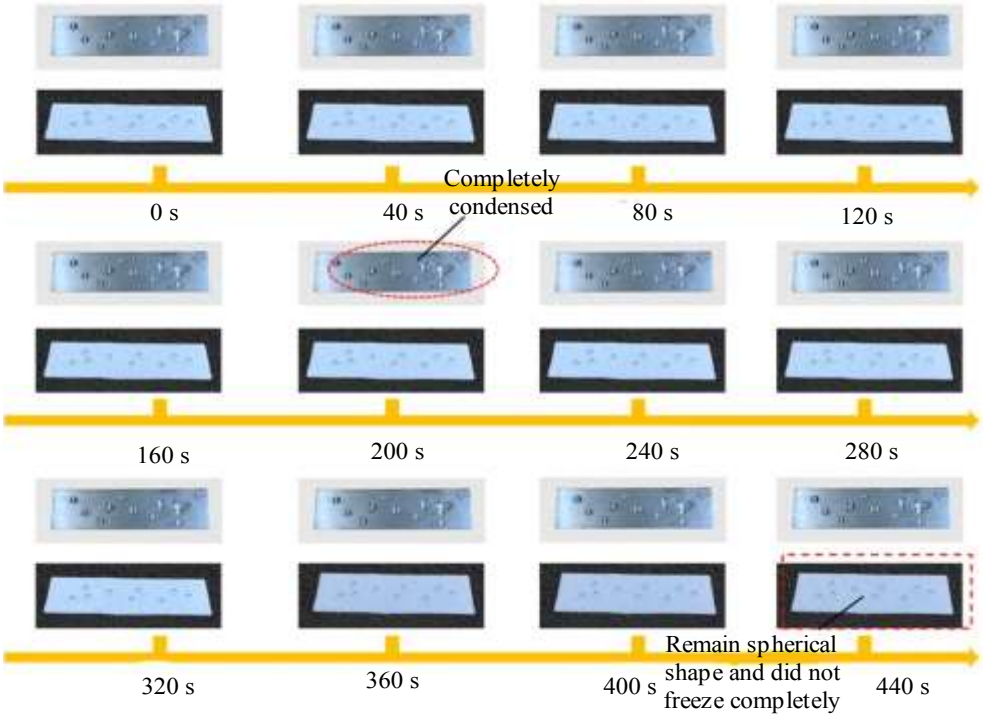

Figure 14. Frozen state between (a) bare S50C CS and (b) 0.40 CaCO3 -0.15ZnO samples at various time intervals.

As depicted in Figure 14, the water droplet on the bare S50C CS surface rapidly adhered and fully froze within 120 seconds. In stark contrast, the droplet on the coated surface maintained a near-spherical morphology and resisted complete freezing for approximately 480 seconds, corresponding to a freezing delay of around 360 seconds.

This significant delay in ice nucleation on the coated sample underscores the superior anti-icing capability imparted by the superhydrophobic surface. The prolonged freezing time is attributed to the combination of low surface energy and the hierarchical micro/nanostructure of the coating, which together trap air pockets and effectively reduce solid–liquid contact, thereby impeding ice formation. Notably, this outstanding anti-icing performance was achieved without the use of any additional anti-freezing agents, demonstrating the coating's intrinsic resistance to ice accumulation under subzero conditions.

Thermal Stability

In many engineering applications, materials often need to withstand high temperatures. For example, materials may be exposed to elevated temperatures during events such as fire accidents or heat-based manufacturing processes. Therefore, it is crucial to evaluate the thermal stability or thermostability of materials to understand how they will perform under such conditions. In this context, the thermostability of the superhydrophobic coating developed in this study was thoroughly tested and assessed, as outlined in Section 2.7 of the methods. The aim was to determine whether the coating could maintain its water-repellent properties after exposure to high temperatures. The material under consideration is a composite coating made of PDMS (Polydimethylsiloxane) and EP (Epoxy Resin), which are combined with micro-$CaCO_3$ (calcium carbonate) and nano-ZnO (zinc oxide) particles. These coatings were subjected to a series of temperature treatments to simulate high-temperature conditions and determine their impact on the coating's properties.

Thermogravimetric analysis (TG) was performed on the individual components of the coating (PDMS and EP) to understand their thermal decomposition behavior. According to previous studies, PDMS and EP are known to be stable at temperatures up to around 400 °C, which means they do not undergo significant decomposition within this temperature range. However, at temperatures higher than 500 °C to 600 °C, these materials start to degrade, which can lead to a loss of their desirable properties. The study also included an experiment where the superhydrophobic coating was subjected to various temperature treatments, ranging from room temperature to as high as 900 °C. The findings, presented in Fig. 15, reveal that the coating retains its original appearance and water-repellent properties when treated at room temperature, 100 °C, 300 °C, and even 500 °C, which suggests that the polymeric matrix (PDMS and EP) does not decompose under these conditions. However, at 700 °C, the coating starts to show visible signs of degradation, turning yellow, and at 900 °C, the coating becomes brown, indicating the onset of decomposition of the polymeric components.

This behavior contrasts with that reported by Qin et al. [35], who studied a similar superhydrophobic coating EP + PDMS@ZnO and found that the cured EP and PDMS components underwent significant weight loss at temperatures of 400 °C and 500 °C, with losses of 56.5% and 68.4%, respectively. In comparison, the superhydrophobic coatings developed in this study show much better thermal stability, with only slight decomposition observed at high temperatures. This is evident from the minimal weight loss during the high-temperature treatment as shown in Table 4.

The ability of the coating to maintain its superhydrophobic properties even after exposure to temperatures as high as 900 °C is a remarkable finding. It suggests that the hierarchical structure of the coating, which includes the micro-$CaCO_3$ and nano-ZnO particles embedded in the PDMS and EP matrix, helps to preserve its water-repellent behavior. The Si-O bonds (silicon-oxygen bonds) in PDMS are known for their thermal stability, which likely contributes to the coating’s ability to resist

decomposition at high temperatures. Furthermore, the incorporation of micro-$CaCO_3$ and nano-ZnO enhances the overall stability of the coating, making it more resistant to thermal degradation. The experimental results demonstrate that even after prolonged exposure to high temperatures, the coating retains its superhydrophobic characteristics, as evidenced by the water droplet's unchanged behavior on the surface. This indicates that the coating could be highly useful in applications where exposure to high temperatures is a concern, such as in industrial settings or environments with fluctuating temperatures.

Buoyancy Performance

The low water adhesion of the superhydrophobic coating enhances the buoyancy of the coated material, as demonstrated by the loading capacity test. As shown in Figure 16, the uncoated glass slide sinks immediately when a load of 10 buttons (approximately 3.67 g) is applied, reaching a maximum load capacity of around 11 buttons (Figure 16a). In contrast, the EP/PDMS@micro-CaCO3/nano-ZnO coated glass slide maintains a stable floating position for over 24 hours, even with a load of 18 buttons (6.24 g) placed on its surface (Figure 16b). This significant improvement in buoyancy further supports the formation of a stable air cushion, which is effectively trapped by the hierarchical surface structure of the coating. The air cushion plays a crucial role in maintaining the buoyancy and stability of the coated sample on water.

Substrate Versatility Test

The surface wettability of the EP/PDMS@micro-CaCO3/nano-ZnO brushed coating was evaluated across various substrates, including fabric, wood, abrasive paper, plastic, and glass, to assess the coating's universal applicability. As depicted in Figure 17, after the EP/PDMS@micro-CaCO3/nano-ZnO coating was applied to these substrates, a consistent and uniform coating layer was observed across all surfaces. This indicates that the coating was successfully applied to each of the diverse substrates, exhibiting excellent water-repellent properties. Despite the distinct chemical compositions and physical characteristics of the materials such as the flexibility of fabric, the rigidity of wood, the smoothness of plastic, and the hardness of glass the coating maintained uniformity across all substrates. This suggests that the EP/PDMS@micro-CaCO3/nano-ZnO coating demonstrates significant versatility, making it suitable for application on a wide range of material surfaces.

Correlation between Microstructure and Performance

The enhanced performance of the superhydrophobic coating can be directly attributed to the synergistic effects of the micro-$CaCO_3$ and nano-ZnO particles embedded within the PDMS matrix. The hierarchical micro-nano structure increases the surface roughness, promoting the formation of air pockets and reducing the contact area between the surface and water droplets. This roughness is critical for achieving superhydrophobicity, as it creates an interface that maximizes the water contact angle while minimizing the sliding angle.

The incorporation of nano-ZnO particles enhances the wear resistance and friction reduction of the coating. ZnO nanoparticles possess self-lubricating properties due to their crystal structure, which facilitates the shearing of the surface during sliding contact, thereby reducing friction and wear. Furthermore, the zinc oxide particles contribute to the coating's mechanical strength by reinforcing the matrix, improving the overall durability and stability of the superhydrophobic surface. The micro-$CaCO_3$ particles, on the other hand, provide additional reinforcement to the coating, preventing mechanical failure and enhancing its wear resistance. The combination of these particles with the PDMS and epoxy matrix results in a highly durable, multifunctional, and corrosion-resistant coating that is well-suited for demanding engineering applications.

Table 4. Weight loss of samples after treatment at various temperature

Temperature (℃)	Room temperature	100	300	500	700	900
Weight loss (g)	0	0	0	0	0.0029	0.0064

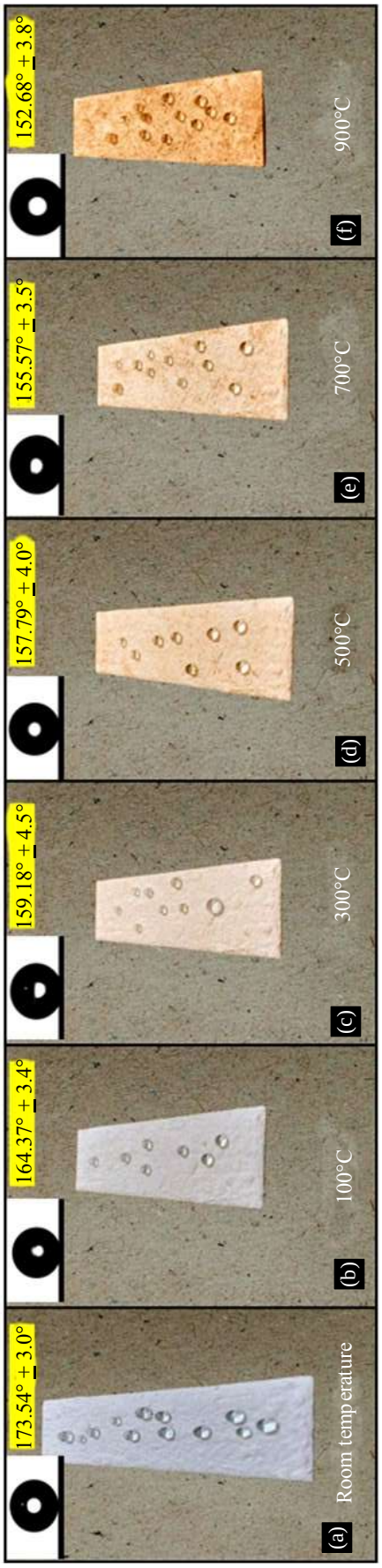

Figure 15. Thermal stability test of 0.40 $CaCO_3$ -0.15ZnO samples heated at different temperatures of (a) room temperature, (b) 100 ◦ C, (c) 300 ◦ C, (d) 500 ◦ C, (e)700 ◦ C, and (f) 900 ◦ C for 10 min.

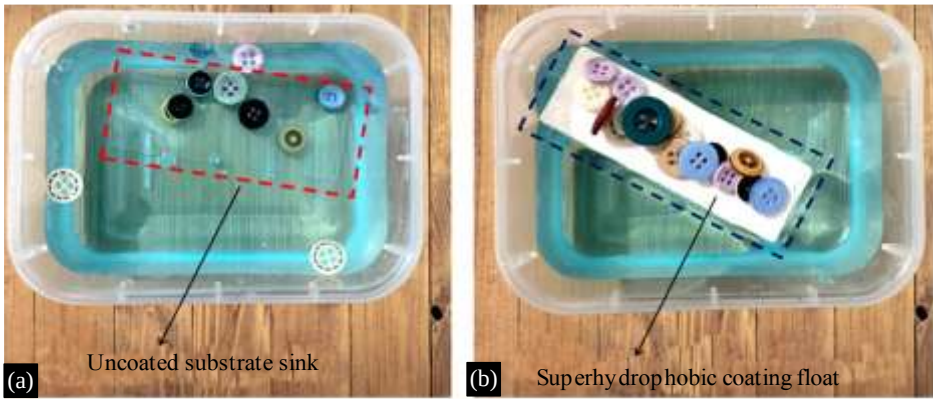

Figure 16. The low water adhesion of the superhydrophobic coating enhances the buoyancy of the coated material as demonstrated by the loading capacity test.

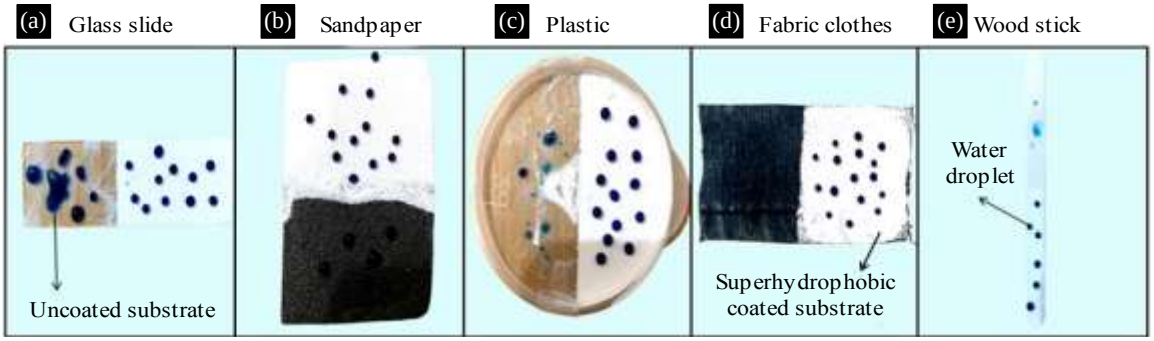

Figure 17. After the EP/PDMS@micro-$CaCO_3$/nano-ZnO coating was applied to these substrates, a consistent and uniform coating layer was observed across all surfaces.

CONCLUSIONS

Conclusions summarize key results and may include any plans for relevant future work. In conclusion, a novel and durable superhydrophobic coating was successfully developed on S50 carbon steel (CS) using a simple, one-step brushing method. This coating integrates micro-sized calcium carbonate ($CaCO_3$) particles, nano-sized zinc oxide (ZnO) particles, PDMS, and epoxy resin (EP), forming a robust protective layer. The optimal mass ratio of micro-$CaCO_3$/nano-ZnO to EP/PDMS is 0.40: 0.15: 0.10: 0.60 which results in a superhydrophobic EP/PDMS@micro-$CaCO_3$/nano-ZnO coating exhibiting a high water contact angle (WCA) of 173.54° ± 2.53° and a low sliding angle (SA) of 1.50° ± 1.12°. The coating demonstrates excellent multifunctionality, including self-cleaning, anti-fouling, anti-icing, thermal stability, and enhanced buoyancy. Electrochemical impedance spectroscopy (EIS) and potentiodynamic polarization tests reveal significantly improved corrosion protection, with corrosion inhibition efficiencies exceeding 99.90%, indicated by elevated Rct and |Z| modulus values, positive shifts in Ecorr, and a substantial reduction in Icorr compared to bare S50 CS. Furthermore, the abrasion test confirms the maintenance of superhydrophobicity even after extended wear, highlighting the coating's remarkable mechanical stability. Tribological testing shows a 76.2% reduction in friction coefficient, demonstrating enhanced tribological performance. The network cross-linking between resin and micro-$CaCO_3$/nano-ZnO particles, coupled with the embedding of surface micro-nano particles, provides excellent wear resistance. This study offers valuable insights for the development of multiscale mixed inorganic particle-based superhydrophobic coatings, making them a promising solution for addressing the corrosion protection challenges faced by traditional carbon steel in real-world applications.

Acknowledgments

This work was supported by the Universiti Malaysia Pahang Internal Grant (RDU210368).

REFERENCES

1. Desai PD, Pawar CB, Avhad MS, More AP. Corrosion inhibitors for carbon steel: A review. *Vietnam J Chem.* 2022;61(1):15–42. doi:10.1002/vjch.202200111.
2. Santulli C, Palanisamy S, Kalimuthu M. Pineapple fibers, their composites and applications. In: *Elsevier eBooks*. 2022. p. 323–346. doi:10.1016/B978-0-12-824528-6.00007-2.
3. Kania H. Corrosion and anticorrosion of alloys/metals: The important global issue. *Coatings.* 2023;13(2):216. doi:10.3390/coatings13020216.
4. Liang Y, Du Y, Zhu Z, Chen L, Liu Y, Zhang L, et al. Investigation on AC corrosion of aluminum alloy sacrificial anode in the artificial simulated seawater environment. *Electrochim Acta.* 2023;446:142002. doi:10.1016/j.electacta.2023.142002.
5. Km S, Praveen B, Devendra BK. A review on corrosion inhibitors: Types, mechanisms, electrochemical analysis, corrosion rate and efficiency of corrosion inhibitors on mild steel in an acidic environment. *Results Surf Interfaces.* 2024;16:100258. doi:10.1016/j.rsurfi.2024.100258.
6. Li G, Ma F, Liu P, Qi S, Li W, Zhang K, et al. Review of micro-arc oxidation of titanium alloys: Mechanism, properties and applications. *J Alloys Compd.* 2023;948:169773. doi:10.1016/j.jallcom.2023.169773.
7. Nazari MH, Zhang Y, Mahmoodi A, Xu G, Yu J, Wu J, et al. Nanocomposite organic coatings for corrosion protection of metals: A review of recent advances. *Prog Org Coat.* 2021;162:106573. doi:10.1016/j.porgcoat.2021.106573.
8. Hu K, Chen Y, Wu D, Tang B, Tao Y, Chen Q. Efficient condensation on spiked surfaces with superhydrophobic and superhydrophilic coatings. *Int J Heat Mass Transf.* 2025;246:127055. doi:10.1016/j.ijheatmasstransfer.2025.127055.
9. Wu Y, Du J, Liu G, Ma D, Jia F, Klemeš JJ, et al. A review of self-cleaning technology to reduce dust and ice accumulation in photovoltaic power generation using superhydrophobic coating. *Renew Energy.* 2021;185:1034–1061. doi:10.1016/j.renene.2021.12.123.
10. Gupta R, Verma R, Kango S, Constantin A, Kharia P, Saini R, et al. A critical review on recent progress, open challenges, and applications of corrosion-resistant superhydrophobic coating. *Mater Today Commun.* 2022;34:105201. doi:10.1016/j.mtcomm.2022.105201.
11. Huang W, Huang J, Guo Z, Liu W. Icephobic/anti-icing properties of superhydrophobic surfaces. *Adv Colloid Interface Sci.* 2022;304:102658. doi:10.1016/j.cis.2022.102658.
12. Fakhri M, Rezaee B, Pakzad H, Moosavi A. Facile, scalable, and low-cost superhydrophobic coating for frictional drag reduction with anti-corrosion property. *Tribol Int.* 2022;178:108091. doi:10.1016/j.triboint.2022.108091.
13. Chu H, Liu Z, Ji T, Yang C, Xu N. Recent advances in the preparation of superhydrophobic coatings based on low-surface-energy modifiers: Diversified properties and potential applications. *Appl Therm Eng.* 2024;251:123591. doi:10.1016/j.applthermaleng.2024.123591.
14. TP R, Philip J. Optimal condition for fabricating mechanically durable superhydrophobic titanium surface by rapid breakdown anodization: Self-cleaning and bouncing characteristics. *Appl Surf Sci.* 2024;585:152628. doi:10.1016/j.apsusc.2022.152628.
15. Wang X, Wang B, Yang W, Zhao Q, Xu Z, Yan W. Fabrication of stable and versatile superhydrophobic PTFE coating by simple electrodeposition on metal surface. *Prog Org Coat.* 2022;172:107090. doi:10.1016/j.porgcoat.2022.107090.
16. Yong J, Yang Q, Hou X, Chen F. Nature-inspired superwettability achieved by femtosecond lasers. *Ultrafast Sci.* 2022. doi:10.34133/2022/9895418.
17. Aziz MHA, Othman MHD, Tavares JR, Pauzan MAB, Tenjimbayashi M, Lun AW, et al. Self-cleaning and anti-fouling superhydrophobic hierarchical ceramic surface synthesized from hydrothermal and fluorination methods. *Appl Surf Sci.* 2022;598:153702. doi:10.1016/j.apsusc.2022.153702.
18. Zhu S, Deng W, Su Y. Recent advances in preparation of metallic superhydrophobic surface by chemical etching and its applications. *Chin J Chem Eng.* 2023;61:221–236. doi:10.1016/j.cjche.2023.02.018.

19. Goutham ERS, Hussain SS, Muthukumar C, Krishnasamy S, Kumar TSM, Santulli C, et al. Drilling parameters and post-drilling residual tensile properties of natural-fiber-reinforced composites: A review. *J Compos Sci.* 2023;7(4):136. doi:10.3390/jcs7040136.
20. He P, Qu J, Li S, Sun R, Huang K, Zhao J, et al. Study on the construction of durable superhydrophobic coatings using simple spray coating method and their underwater drag reduction performance. *Colloids Surf A.* 2024;701:134858. doi:10.1016/j.colsurfa.2024.134858.
21. Wang Y, Ge-Zhang S, Mu P, Wang X, Li S, Qiao L, et al. Advances in sol–gel-based superhydrophobic coatings for wood: A review. *Int J Mol Sci.* 2023;24(11):9675. doi:10.3390/ijms24119675.
22. Liu M, Wang S, Jiang L. Nature-inspired superwettability systems. *Nat Rev Mater.* 2017;2(7). doi:10.1038/natrevmats.2017.36.
23. Peng J, Yuan S, Geng H, Zhang X, Zhang M, Xu F, et al. Robust and multifunctional superamphiphobic coating toward effective anti-adhesion. *Chem Eng J.* 2021;428:131162. doi:10.1016/j.cej.2021.131162.
24. Karuppiah G, Kuttalam KC, Palaniappan M, Santulli C, Palanisamy S. Multiobjective optimization of fabrication parameters of jute fiber/polyester composites with egg shell powder and nanoclay filler. *Molecules.* 2020;25(23):5579. doi:10.3390/molecules25235579.
25. Aruchamy K, Karuppusamy M, Krishnakumar S, Palanisamy S, Jayamani M, Sureshkumar K, et al. Enhancement of mechanical properties of hybrid polymer composites using palmyra palm and coconut sheath fibers: The role of tamarind shell powder. *BioResources.* 2024;20(1):698–724. doi:10.15376/biores.20.1.698-724.
26. Palanisamy S, Mayandi K, Dharmalingam S, Rajini N, Santulli C, Mohammad F, et al. Tensile properties and fracture morphology of *Acacia caesia* bark fibers treated with different alkali concentrations. *J Nat Fibers.* 2022;19(15):11258–11269. doi:10.1080/15440478.2021.2022562.
27. Yap SW, Johari N, Mazlan SA, Ahmad SNAS, Arifin R, Hassan NA, et al. Superhydrophobic zinc oxide/epoxy coating prepared by a one-step approach for corrosion protection of carbon steel. *J Mater Res Technol.* 2023;25:5751–5766. doi:10.1016/j.jmrt.2023.07.013.
28. Yang H, Dong Y, Li X, Gao Y, He W, Liu Y, et al. Development of a mechanically robust superhydrophobic anti-corrosion coating using micro-hBN/nano-Al_2O_3 with multifunctional properties. *Ceram Int.* 2024. doi:10.1016/j.ceramint.2024.11.027.
29. Wang Y, Wu M, Wang J, Huang J, Yang K, Miao X, et al. The addition of SiO_2–GO hybrid material enhanced the tribological properties of fluorocarbon resin in marine corrosive environments. *Mater Today Commun.* 2024;39:108676. doi:10.1016/j.mtcomm.2024.108676.
30. Farh HMH, Seghier MEAB, Zayed TA. A comprehensive review of corrosion protection and control techniques for metallic pipelines. *Eng Fail Anal.* 2022;143:106885. doi:10.1016/j.engfailanal.2022.106885.
31. McGuire SC, Ebrahim AM, Hurley N, Zhang L, Frenkel AI, Wong SS. Reconciling structure prediction of alloyed, ultrathin nanowires with spectroscopy. *Chem Sci.* 2021;12(20):7158–7173. doi:10.1039/D1SC00627D.
32. Ayrilmis N, Kanat G, Avsar EY, Palanisamy S, Ashori A. Utilizing waste manhole covers and fibreboard as reinforcing fillers for thermoplastic composites. *J Reinf Plast Compos.* 2024;44(17–18):1108–1118. doi:10.1177/07316844241238507.
33. Barthwal S, Lim S. A durable, fluorine-free, and repairable superhydrophobic aluminum surface with hierarchical micro/nanostructures and its application for continuous oil–water separation. *J Membr Sci.* 2020;618:118716. doi:10.1016/j.memsci.2020.118716.
34. Bhaumik S, Chowdhury D, Batham A, Sehgal U, Ghosh C, Bhattacharya B, et al. Analysing the frictional properties of micro-dimpled surface created by milling machine under lubricated condition. *Tribol Int.* 2020;146:106260. doi:10.1016/j.triboint.2020.106260.
35. Qin X, Kong L, Wang J, Liu M, Lu S, Wang X, et al. Double-layer with electroactive and superhydrophobicity based on polymer nanotubes to improve robustness and anti-corrosion performances. *Chem Eng J.* 2024;488:150928. doi:10.1016/j.cej.2024.150928.

